

University of Colorado Boulder
Department of Computer Science

The Roles of Inertia and Stability in Power Systems

Samantha Molnar

February 2019

Abstract

Power systems today are undergoing extreme changes with the integration of renewable generation sources such as solar and wind. With these new technologies come new challenges. Traditional generation sources, such as coal and natural gas, provide inertial support, which helps maintain system stability when an outage occurs. However, solar and wind generation do not, on their own, provide this support, which potentially makes the system more vulnerable to failures. The effect on stability as power engineers introduce more renewables into the generation mix remains an open question. I start to address this question by studying system dynamics by changing two aspects of inertia: the *total* system inertia and the *structural distribution* of inertia. I show how both of these aspects of inertia are important to power system dynamics. Specifically, I measure the frequency dynamics of cascading failure simulations under various inertia scenarios.

Contents

Abstract	i
1 Introduction	1
2 Power Systems Background	4
2.1 Structure and Organization of Power Systems	4
2.2 Power Flow Equations	6
2.3 Power System Dynamics	11
2.3.1 Inertia	14
2.4 Power System Stability	15
2.4.1 Frequency and Rotor Angle Stability Metrics	17
2.5 Cascading Failures in Power Systems	20
3 Role of Power System Inertia in Cascade Events	24
3.1 Experimental Setup	26

3.2 Preliminary Results	28
4 Conclusion	38
Bibliography	39

List of Figures

1.1	Left: Projected growth of fuel types, based on current trends in the energy market. Right: Amount of greenhouse gas emissions by energy fuel type, based on projected electricity consumption. Figures from the Energy Information Administration 2018 Annual Energy Outlook [2].	2
2.1	The interconnections of North America. Although interconnections are connected, they can function individually from each other. Image from [40]. . .	5
2.2	Basic illustration of an electric generator with the mechanical and electromagnetic phenomena labeled. Based on figures in [49] and [57].	12
2.3	An example of a frequency deviation after a loss of generation, with relevant frequency measures labeled.	18
2.4	An example of a rotor angle time series with acceptable (black line), and unacceptable (red line) behavior.	19
3.1	Plot of the power system test cases for the proposed experiments. Generators are marked in green; all other buses are in red.	27

3.2 Set of outcomes that can occur after an initial failure. (I) No other failures occur and the network remains connected. (II) $N - 1$ contingency disconnects the network, but no other failures occur. (III) A cascade of failures occurs but the network remains connected. (IV) A cascade of failures occurs and the network disconnects. The sizes of the circles do not indicate the number of scenarios that belong in each category.	29
3.3 Frequency dynamics of the Illinois 200 bus test case for an outage that falls into category (I).	30
3.4 Average over all category (I) contingencies of the maximum RoCoF for the Illinois 200 bus test case.	31
3.5 Frequency dynamics for each category (I) contingency as a function of inertia for the Illinois 200 bus test case. For clarity, a darker line color indicates a larger magnitude.	31
3.6 Impact of inertia distance on frequency deviations for category (I) contingencies of the Illinois network. The colored points in the left plot correspond to the colored edges in the right plot.	32
3.7 Frequency dynamics for the category (III)	34
3.8 Category (II) time series and frequency dynamics for the Illinois test case.	35
3.9 Category (IV) time series and frequency dynamics for the Illinois test case.	36

Chapter 1

Introduction

Power systems today are undergoing significant changes in an effort to make them more sustainable and environmentally friendly. This is due to the fact that electricity is one of the largest contributors to greenhouse gases in the U.S., only slightly below transportation [18]. Until very recently, the majority of these emissions were due to the significant use of coal as a fuel source for electricity, as seen on the right side of Figure 1.1. However, based on the lowering price of natural gas and variable renewable generation (VRG), such as wind and solar photovoltaics (PV), it is expected that VRG will contribute at least as much energy as coal by the year 2050¹ (see left panel of Figure 1.1) [2].

These forecasts indicate a need to understand how VRG will reshape power-system operations. Power systems function based on a delicate balance between the generation and consumption of electricity. This balance must be maintained at all time scales, from seconds to days and everything in between. Managing this balance is well understood when the generation sources have a controllable fuel source, such as coal or natural gas. But these well-established procedures have been disrupted by VRG; renewable resources are not controllable in the same ways as traditional fuel sources. Specifically conventional generation

¹Note: These projections do not consider the Clean Power Plan implemented in 2014.

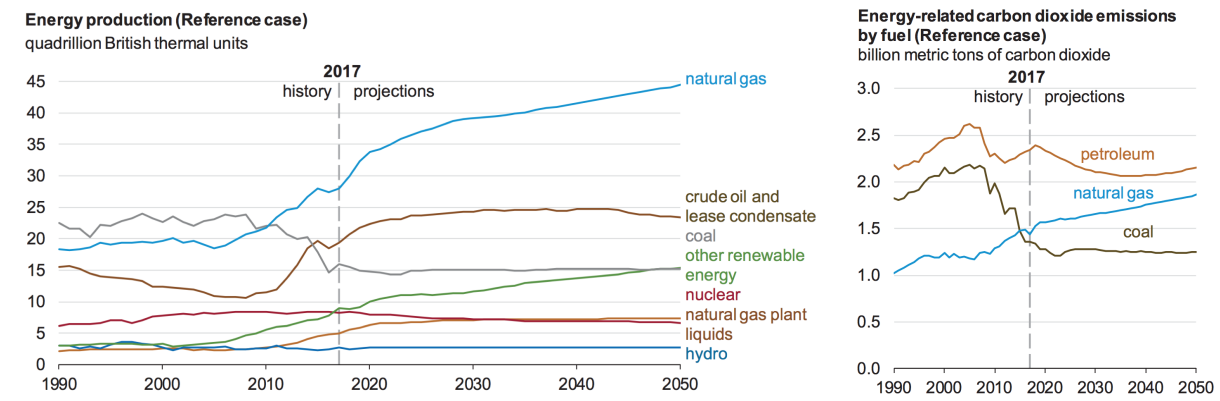


Figure 1.1: **Left:** Projected growth of fuel types, based on current trends in the energy market. **Right:** Amount of greenhouse gas emissions by energy fuel type, based on projected electricity consumption. Figures from the Energy Information Administration 2018 Annual Energy Outlook [2].

sources, such as gas or coal, are dispatchable, meaning the power output is controllable. On the other hand, wind and solar resources are determined by weather patterns, and thus uncontrollable. This issue means there need to be more grid flexibility options to compensate for this lack of control. Over the past decade, innovative solutions have emerged: storage technologies allow us to use solar power at night; aggregation of wind turbines helps smooth the intermittency of wind power. Cost incentives and increases in grid flexibility help explain rapid VRG adoption across the world. For example, in 2017 the Texas power system had large amount of wind generation. Wind energy production surpassed nuclear that year, at one point reaching a 54% instantaneous penetration [42].

As VRG replaces more thermal generation sources, new questions arise regarding grid stability. Traditional generators create electricity using large spinning rotors. When a power imbalance occurs, generators spin faster or slower to restore balance. This immediate response is determined by the *inertia* of each generator. However, VRGs do not have this spinning support, or inertia. Thus, as VRG levels increase, the natural balancing forces provided by and for traditional generators will decrease. It is this decrease in *inertial support* that has become a prominent issue in the power systems community, and on which I will focus.

The goal of this work is to characterize how inertia impacts system responsiveness to imbalances of electric power. As a first step, I test how system stability changes based on the *total* inertia and the *structural distribution* of inertia. I show that a decrease in total inertia has a non-linear impact on power system stability. Furthermore, I hypothesize that the location of low-inertia generators in the network has a strong influence on which perturbations create severe instabilities. These questions and results are discussed further in Chapter 3. The next chapter discusses the necessary terminology and mathematical foundations for that discussion.

Chapter 2

Power Systems Background

This chapter provides background regarding the terminology and modeling of power systems. Each section gives a brief introduction to material that is covered in numerous textbooks. The chapter begins with a discussion of the terminology and organizational structure of the U.S. power system, followed by modeling foundations. The final section describes cascading failures and a detailed description of the failure model used to study inertia in power system dynamics.

2.1 Structure and Organization of Power Systems

The basic components of power systems highlight key differences in its organization and structure. A power system consists of a generator and a load, with power lines connecting the two. Generators create electricity, while loads consume it. Based on distinct physical properties, the power systems community generally divides power lines into two networks: the transmission system and the distribution system. The transmission system is a mesh network that consists of high voltage power lines exchanging and delivering power over large regions. The distribution system tends to be a tree-like network which delivers power from

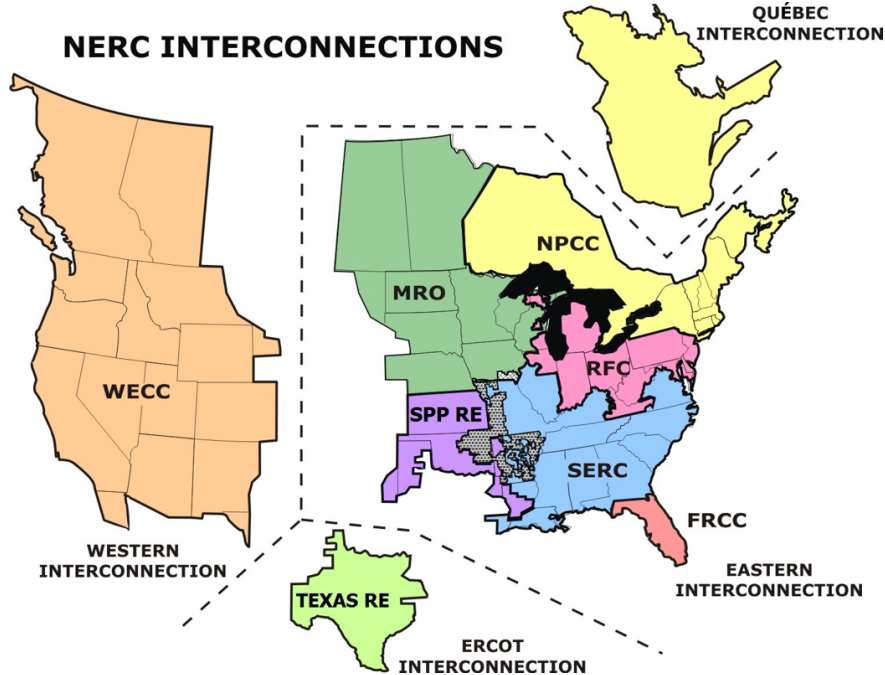


Figure 2.1: The interconnections of North America. Although interconnections are connected, they can function individually from each other. Image from [40].

the transmission system to consumers. This work focuses on transmission systems because of the dynamical challenges that have arisen from replacing traditional generation sources with VRG.

There are numerous entities involved in the control, regulation, and operation of transmission systems. In North America, there are two agencies that regulate power systems: the Federal Energy Regulatory Commission and the North American Electric Reliability Corporation. As the name may suggest, the Federal Energy Regulatory Commission (FERC) oversees energy markets, interstate energy exchanges, and quality standards [10]. The North American Electric Reliability Commission (NERC) creates and enforces statutes to ensure FERC standards are met [39]. NERC oversees four interconnections in the United States, as indicated by the dotted lines in Figure 2.1. In a given interconnection, all electric utilities are tied together, such that the stability of one depends on all the others. While each interconnection may exchange electricity, they can all function as individual power systems. Within each interconnection exist regional entities that carry out NERC standards. These

regional entities consist of multiple transmission system operators, generation providers, and distribution systems.

The organizations outlined in this section have a responsibility to define, study, and test the models and equations relevant to the secure operation of power systems. Often, the amount of mathematical detail varies based on the task at hand. For example, utility companies decide which generators to turn on using the power flow equations. On the other hand, interconnections evaluate generation expansion plans based on system transient dynamics. This work focuses on the dynamics of transmission system under various generation scenarios. Thus, the rest of this chapter focuses on these mathematical descriptions relevant to this work.

2.2 Power Flow Equations

Often, power transmission grids are first described as a steady-state system that defines how electricity flows from generators to loads. The equations that describe the steady-state of the system are referred to as the power flow equations (PFE) [7]. Specifically, the PFE solve for the electric current on every line and the voltage at every node. There are two types of electrical current: alternating current (AC) and direct current (DC). As power systems began to grow in size, there were debates over which was best to use¹. The debate involved efficiency and cost. It is more efficient to send power at a high voltage because it decreases the power lost through transmission lines. While high voltages *can* be achieved using DC, lowering the voltage to a safe level for consumers is still cheaper using an AC voltage transformer [57]. Thus, utility companies built transmission systems with AC power lines. As a consequence, power system modeling and analysis can be quite technical and intimidating. This section starts from a basic understanding of circuits and builds to the

¹ “Debates” is perhaps putting it lightly; it is more commonly referred to as the War of the Currents. I highly recommend *Empires of Light* by Jill Jonnes for more information.

AC power flow equations (ACPFE).

The PFE describe physical quantities for buses (nodes) and lines (edges). There are three types of buses: generators, loads, and intermediaries. In this work, the set N of all buses has a cardinality of $|N| = n_b$. Generator buses are represented by the set G with cardinality $|G| = n_g$, and load buses by the set D with cardinality $|D| = n_d$. It is common practice in the power systems community to only represent generator and load buses, and this work adheres to that standard [15]. Finally, two buses i and j are connected if there exists a line $\ell_{i,j}$ in the set of lines L . There are $|L| = n_l$ lines in the network. The PFE can be built up starting from foundational knowledge of circuits.

Ohm's law defines the relationship between current (I), voltage (V), and resistance (R) for a simple DC circuit (Equation 2.1a).

$$I = \frac{V}{R} \quad (2.1a)$$

When inductors are present, the AC form of Ohm's law applies (Equation 2.1b); hence voltage (\bar{V}), current (\bar{I}), and impedance (\bar{Z}) are complex quantities.

$$\bar{I} = \frac{\bar{V}}{\bar{Z}} \quad (2.1b)$$

Specifically, the complex voltage and current are phasors with magnitudes and angles (Equations 2.2).

$$\bar{I} = |I| (\cos(\theta) + \mathbf{j} \sin(\theta)) \quad (2.2a)$$

$$\bar{V} = |V| (\cos(\delta) + \mathbf{j} \sin(\delta)) \quad (2.2b)$$

The physical parameters of a transmission line are quantified by the impedance \bar{Z} , where the real part is the resistance (R), and the imaginary part is the reactance (X) of the line (Equation 2.3).

$$Z = R + \mathbf{j}X \quad (2.3)$$

Resistance quantifies the opposition to the flow of current, while reactance quantifies the opposition to the *change* in current or voltage.

Although impedance is defined by well-known quantities, it is common practice to instead use the *admittance* value of a transmission line. Admittance is simply the inverse of impedance (Equation 2.4).

$$Y = \frac{1}{Z} = G - jB \quad (2.4)$$

Similarly, the conductance G is the inverse of resistance, and the susceptance B is the negative inverse of reactance. The admittance of a line is used for computational efficiency. Solving the PFE for a transmission system requires matrices, and the admittance matrix is sparse while the impedance matrix is dense. In this chapter, bold symbols are used to represent matrices.

Using the admittance substitution and matrix notation, Equation 2.1b is rewritten in Equation 2.5.

$$\mathbf{I} = \mathbf{Y}\mathbf{V} \quad (2.5)$$

Then, the total current at bus i is the sum of the currents of all lines connected to that bus.

$$I_i = \sum_{j=1}^{n_b} Y_{ij} V_i$$

This is an exact statement of Kirchhoff's current law.

Finally, the last equation necessary to derive the PFE relates electric power to current and voltage. This relationship is defined in Equation 2.6, where $*$ denotes a complex conjugate.

$$I_i = \sum_{j=1}^{n_b} Y_{ij} V_j = \frac{S_i^*}{V_i^*} \quad (2.6)$$

Complex power S has a real component and an imaginary component, as shown in Equation

2.7.

$$S_i^* = P_i + \mathbf{j}Q_i \quad (2.7)$$

The real component P_i is referred to as the *real power*, and the imaginary component Q_i is referred to as the *reactive power*. Physically, real and reactive power are different types of energy that are created and consumed by different electrical components. Resistive components, such as light bulbs, consume real power while inductive components, such as air conditioners, consume both real and reactive power. There are also mathematical reasons for separating complex power into its real and imaginary parts, which will be explained later in this section.

The final step in deriving the PFE substitutes the phasor definition of voltage, Equation 2.2, into Equation 2.6. A helpful definition is $\delta_{ij} = \delta_i - \delta_j$ for the difference in voltage angles between bus i and bus j .

$$S_i^* = P_i + \mathbf{j}Q_i = |V_i| \sum_{j=1}^{n_b} |V_j| (G_{ij} - \mathbf{j}B_{ij}) (\cos(\delta_{ij}) + \mathbf{j} \sin(\delta_{ij}))$$

This form easily separates into real and imaginary parts, and completes the PFE derivation.

$$P_i = |V_i| \sum_{j=1}^{n_b} |V_j| (G_{ij} \cos(\delta_{ij}) + B_{ij} \sin(\delta_{ij})) \quad (2.8a)$$

$$Q_i = |V_i| \sum_{j=1}^{n_b} |V_j| (G_{ij} \sin(\delta_{ij}) - B_{ij} \cos(\delta_{ij})) \quad (2.8b)$$

Equations 2.8a - 2.8b describe the *alternating current power flow equations* (ACPFE). A few parameters are given *a priori* to solve this system of equations. By convention, the real power ($P_i = P_g$), and voltage magnitude ($|V_i| = |V_g|$) of each generator is given, while the real power ($P_i = -P_d$) and reactive power ($Q_i = -Q_d$) is given for each load² [41]. Lastly,

²The negative here means that real and reactive power are consumed at these nodes

a reference node— the “slack” node— is defined for the system such that its voltage angle is always zero ($\delta_i = 0$). Generally, the slack node is chosen to be the largest generator [7].

The ACPFE can be difficult to solve in practice, for reasons discussed momentarily. Often, these equations are simplified for quick solutions, or for problems that require solving the PFE a large number of times [47]. This simplification is called the DC approximation, where “DC” means decoupled, **not direct current**. For this approximation, the following assumptions are made:

- $|\delta_{ij}|$ is small such that $\sin(\delta_{ij}) \approx \delta_{ij}$
- For every line, the resistance is much smaller than the reactance, which means $G_{ij} \approx 0$ and $B_{ij} \approx \frac{-1}{X_{ij}}$
- $|V_i| \approx 1, \quad \forall i \in N$
- $\forall i \in N \ Q_i$ is constant

The appropriate use of the DC approximation is a long-standing debate in the power systems community. Generally, the assumptions listed above are valid when the system is operating near a steady state [44]. When there are significant disturbances, though, there can be a discrepancy between the DC approximation and the ACPFE; solving the ACPFE in this situation is non-trivial [53]. Often, the solutions can diverge, which requires an exploration of multiple initial conditions to obtain convergence. Needless to say, a strict rule has not emerged from the community. The proposed research requires numerous simulations over a multitude of power system scenarios. The DC approximation is used in this work to keep computational times down.

The PFE solve for the equilibrium point, or steady-state, of a system. It is important to understand if a steady-state is a feasible solution given a number of physical constraints, such as line limits. However, the PFE only determine *what* the equilibrium points are, they

do not define how the system behaves near the equilibrium, nor how a system behaves after a perturbation [57]. My research interests specifically involve the latter questions, which makes a background on power system dynamics necessary.

2.3 Power System Dynamics

Power system dynamics refers to the *dynamical* equations associated with the motion of the machines—generators and loads—in a system. In general, generator dynamics are consistent across dynamical models; usually, models are distinguished by the load dynamics [41]. I begin with a brief description of the physical phenomena occurring during power generation, followed by the equation of motion. This naturally flows into the equation of motion for loads.

Generators produce electricity by converting *mechanical* energy into *electrical* energy [49]. The essential phenomenon that generators are utilizing is defined by Faraday’s law, which states that a changing magnetic field induces an electric field [23]. Figure 2.2 illustrates the basic process of power generation. First, steam or falling water induces a torque on the turbine, producing mechanical energy. The shaft, which has a wire attached to it, turns with the turbine. The wire is in a magnetic field, so when it turns this causes an electric current to flow through it. The electric power a generator produces is exactly related to the speed at which the turbine rotates: the faster the turbine spins the more power it produces.

The equation of motion for a generator relates the rotational speed and acceleration of the turbine to the power output. It is often referred to as the *swing equation*.

$$M_g \dot{\omega}_g + D_g \omega_g = P_{m_g} - P_{e_g}, \quad (2.9)$$

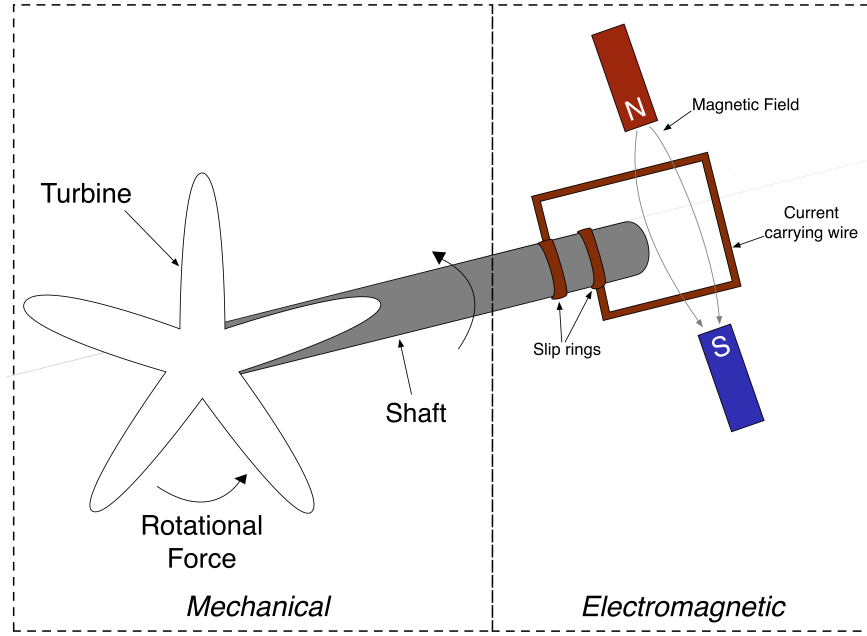


Figure 2.2: Basic illustration of an electric generator with the mechanical and electromagnetic phenomena labeled. Based on figures in [49] and [57].

$$\dot{\delta}_g = \omega_g - \omega_R, \quad \forall g \in G$$

Equation 2.9 is a statement of Newton's second law. The constants M_g and D_g , the inertia and damping constants, are based on the type and mechanical specifications of the generator. The importance of the inertia constant is discussed in more detail in Section 2.3.1. The turbine angle, δ_g , and angular speed, ω_g , are defined with respect to a rotating reference frame ω_R (the slack bus). P_{m_g} is the mechanical power input to the machine's rotor, and P_{e_g} is the electric power output of the generator; thus $P_{m_g} - P_{e_g}$ describes how much energy is stored in the rotating armature of the generator [5].

Based on Equation 2.9, there are two variables that can change the speed of rotation of a generator. The first is by changing P_{m_g} , which is achieved by changing the amount of fuel that is burned. The second is by changing P_{e_g} which is achieved by a change in power consumption or flow in the network. The second point can be seen more clearly by substituting in the

power flow equations for P_{e_g} .

$$\dot{\omega}_g = -\frac{D_g}{M_g}\omega_g + \frac{1}{M_g}(P_g - \sum_{\forall i \notin G} b_{gi} \sin \delta_{gi}), \quad \forall g \in G \quad (2.10)$$

Interestingly, Equation 2.10 takes on the form of a second-order Kuramoto oscillator, which helped spark a broader interest in power system dynamics [14][3]. More detailed descriptions of generator dynamics include the governor, which is responsible for controlling the generator frequency, and the excitation system, which controls the internal voltage magnitude of the generator. This work is concerned with the natural response of a generator to system disturbances without any control or support mechanisms. Therefore, the more detailed descriptions of generator dynamics are not used.

A key component of the dynamical model is the representation of load nodes. In this work the *structure preserving* model is used. This means that instead of modeling loads as static variables they evolve dynamically as first-order oscillators [41]. Thus, a load node is modeled by Equation 2.11 where D_i is the damping constant that describes the frequency dependence of the node.

$$\dot{\delta}_i = -\frac{1}{D_i}(P_i + \sum_{\forall j \in N} b_{ij} \sin \delta_{ij}), \quad \forall i \in L \quad (2.11)$$

The primary goal of this work is understanding the change in system dynamics as traditional synchronous generation (SG) is replaced by non-synchronous generation (*i.e.* VRG). One consequence of this change is less reliable and predictable power sources. But, a less studied aspect involves the change in system response when there are disturbances. This change is due to the differences in machine inertia, discussed in the next section.

Generation Type	Base Power Rating (MVA)	H (sec.)	M (MW · s)
Nuclear	1410 – 1504	3.8 – 4.24	5344 – 6530
Coal	194 – 1120	2.9 – 4.5	863 – 3158
Gas CT	7 – 235	1 – 12.5	22 – 1288
Gas Steam	14 – 887	1 – 5.4	13 – 2216
Gas CC	25 – 1433	1.1 – 9	97 – 8765
Hydro	10 – 70	2 – 3	19 – 1133

Table 2.1: Table of inertia values for various generation types in the ERCOT interconnection. Values obtained from [20].

2.3.1 Inertia

As discussed earlier, a generator is a spinning rotor where the acceleration or deceleration determines its change in power output. The constant M_g is often referred to as the inertia constant, but it is perhaps better to refer to it as the inertia *coefficient* for now. The inertia *constant* can also refer to the value H_g , which has units of seconds. H_g is based on the shape and size of the rotor, and it quantifies the amount of time a generator can provide its rated maximum power, S_g , purely from the energy stored in the spinning turbine. These constants are all related based on Equation 2.12 [30].

$$M_g = \frac{2S_g H_g}{\omega_R} \quad (2.12)$$

M_g is really a description of the maximum amount of kinetic energy that can be stored in the rotor of a generator. Table 2.1 provides some typical values of the inertia constant H and the inertia coefficient M_g based on the generation type. Interestingly, generation types that are most likely to be replaced by VRG, such as coal, tend to have high inertia constants.

Lastly, it is useful to define the *total system inertia*. Often this is used when aggregating models for generators, but I use it as an independent variable in my experiments, discussed more in Chapter 3. Equation 2.13 defines the total system inertia as a weighted sum of the

inertia constant of every generator [55].

$$H_{tot} = \frac{\sum_{g=1}^{n_g} H_g S_g}{\sum_{g=1}^{n_g} S_g} \quad (2.13a)$$

$$M_{tot} = \sum_{g=1}^{n_g} M_g \quad (2.13b)$$

Unlike traditional (synchronous) generation, VRG must be connected to a transmission system through a power electronic device called an inverter to protect and control VRG equipment. Typically multiple VRG are connected to one inverter. This simplifies control and increases power quality [33]. Fundamentally, inverters convert the current provided by VRG to AC current that matches the grid [54]. Due to the fact that there are no spinning parts of an inverter, there is no natural inertia associated with renewable generation. In terms of the modeling equations, this simply means that $M_g = 0$ and the equation of motion for renewable generators then becomes equivalent to Equation 2.11 for loads³.

An important point about generator inertia is that it dictates the *immediate* response of a generator to a power imbalance: the instantaneous reaction to an increase or decrease in P_{eg} . However, due to the AC-DC inverter coupling, renewable generators do not have this natural reaction to power imbalances⁴. This fact can have important consequences on power system stability. As such, the next section briefly introduces power system stability to further explain these concerns.

2.4 Power System Stability

Broadly speaking, stability is defined as on the ability of a dynamical system to return to an equilibrium state following a disturbance [26]. For power systems, there are three categories

³In Equation 2.11, the damping D_i and power P_i terms determine whether i is a generator or load node

⁴Unless the inverter has special controls which create “virtual inertia” [46]

of stability found in the literature: voltage stability, frequency stability, and rotor angle stability [25]. Each of these categories have a different driving force, even if they co-occur. I outline the basic concepts of each category, but pay special attention to frequency and rotor angle stability, as these are most influenced by power system inertia.

Voltage stability is quantified by the ability of a system to maintain bus voltages at acceptable levels. It is a measure of the balance between reactive power supply and demand [1]. One particular type of voltage instability is fault-induced delayed voltage recovery. When a fault (failure) is cleared from the system it causes low voltages at nearby buses. These low voltages raise the reactive power requirement of motors, particularly air-conditioning units. When the reactive power cannot be met, the AC units stall, causing them to need 5-6 times the pre-contingency reactive power [37]. This, in turn, decreases voltages even further and can lead to large spread failure—including voltage collapse, when the voltage of the nodes start to drop first slowly and then quickly until the system cannot recover [27]. Although concerns about voltage instabilities have grown over the years, in part due to large amounts of distributed solar, this work is primarily focused on issues related to inertia which most directly affects frequency and rotor angle stability.

Frequency stability and rotor angle stability are dependent upon generator dynamics. Frequency stability is the ability of the system to maintain a frequency within a specified margin after an upset that causes an imbalance between real power generation and consumption [38]. When generation is less than consumption, there is a frequency drop, and vice versa when generation is greater than the load. If the frequency deviates too far from the nominal value, equipment and/or load is disconnected to avoid damage. The severity of frequency excursions is discussed further in Section 2.4.1.

The system frequency is a global measure of power balance, even though its value can vary throughout the network topology. The frequency of an interconnection is related to the

inertia and rotor speed of each generator according to Equation 2.14.

$$\omega_{COI} = \frac{\sum_{g=1}^{n_g} M_g \omega_g}{\sum_{g=1}^{n_g} M_g} \quad (2.14)$$

$$\omega = 2\pi f$$

This is commonly referred to as the Center of Inertia (COI) frequency and is essentially a weighted average of the rotor speeds. Equation 2.14 is simple enough to compute for simulations; in practice, operators measure the frequency at some relevant bus in the network.

Closely related to frequency stability is rotor angle stability, which is defined by the individual oscillations of a generator. When a generator loses synchrony with others due to an instability, the rebalancing forces from other generators will usually restore it to the proper oscillation speed and phase. This depends on the ability of the system to restore the equilibrium between the mechanical and electromagnetic torque of the generator. The system becomes unstable when it cannot absorb the kinetic energy caused by the differences in rotor speeds [25][57].

2.4.1 Frequency and Rotor Angle Stability Metrics

As mentioned in Section 2.1, NERC creates and enforces minimum operating requirements for interconnections and balancing authorities. This section defines the relevant metrics for frequency and rotor angle stability.

There are a few metrics for frequency stability. Consider a power system with a small amount of VRG but is dominated by traditional generation sources. After a loss of generation, the frequency of the system resembles Figure 2.3. Three different metrics are typically used to quantify the severity of such a frequency excursion. The first is the frequency NADIR,

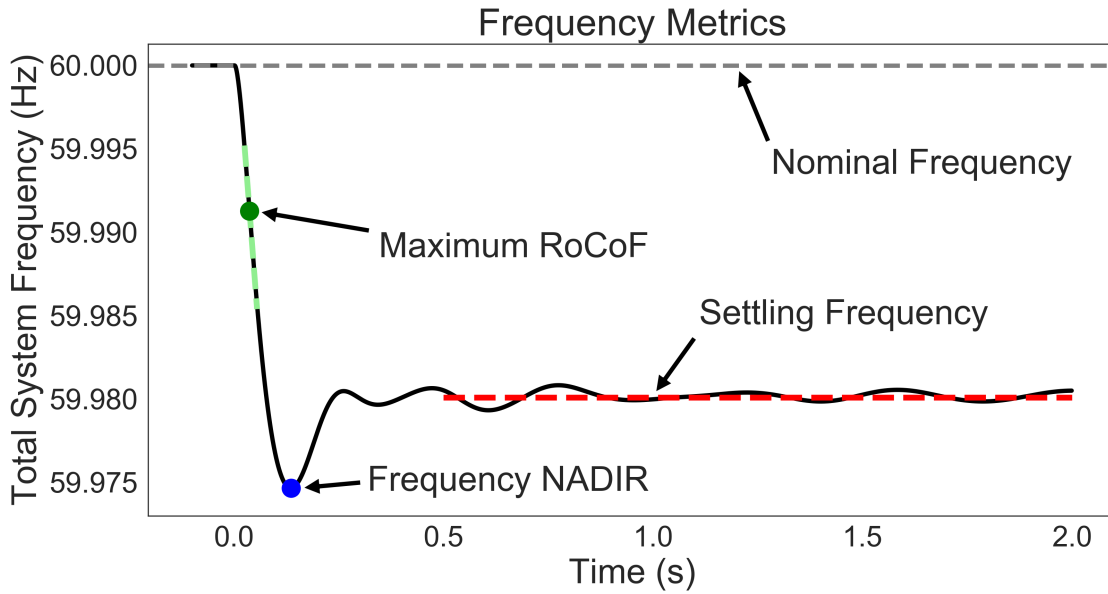


Figure 2.3: An example of a frequency deviation after a loss of generation, with relevant frequency measures labeled.

denoted by a blue point in Figure 2.3: the largest frequency deviation from the nominal value. Each interconnection has a specified Frequency NADIR where under-frequency load shedding (UFLS) occurs: eastern and western interconnections are 59.5 Hz, and ERCOT is 59.3 Hz [38]. Related to the frequency NADIR is the maximum rate of change of frequency (RoCoF), denoted by the green point in Figure 2.3: the steepest slope of the frequency time series. NERC sets RoCoF limits by analyzing the largest generation contingency that could occur in each interconnection. Internationally there are specific set points for this, from as small as 0.5Hz/s in Ireland, to as high as 2.5Hz/s in Denmark [48]. Finally, the settling frequency is denoted by the dashed red line in Figure 2.3. This value indicates the effectiveness of generators to stabilize system frequency [56].

As mentioned in Section 2.4, rotor angle stability is closely related to frequency stability. Rotor angle stability is based on the damping capabilities of each individual generator, which in turn determine whether it will remain synchronized with the system. NERC does not have a specific method for determining rotor angle stability, but some regional entities

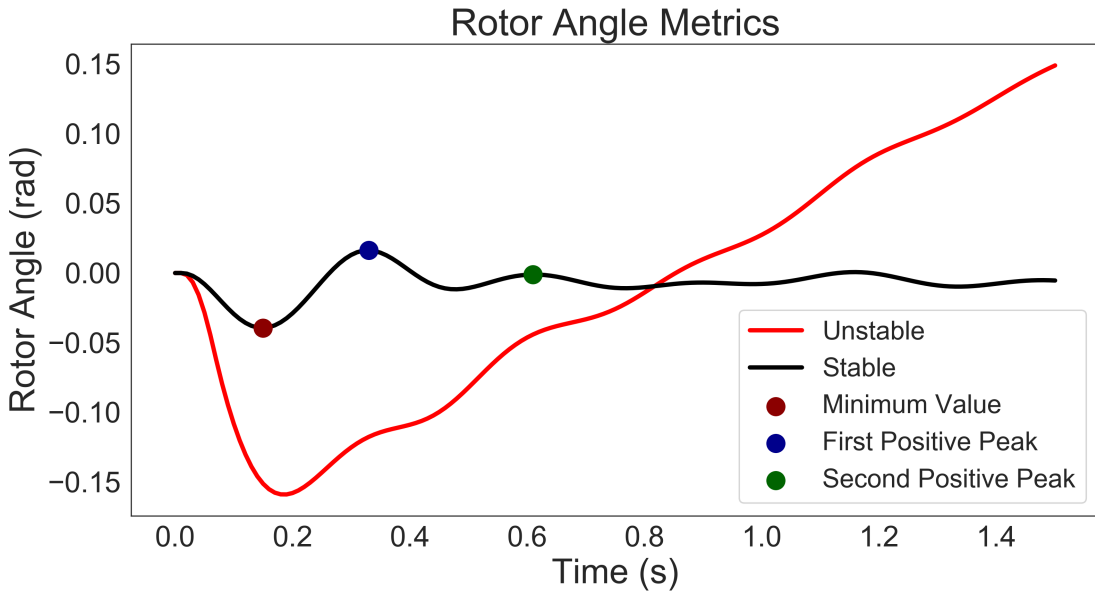


Figure 2.4: An example of a rotor angle time series with acceptable (black line), and unacceptable (red line) behavior.

do explicitly calculate this for specific generating units [45]. Figure 2.4 shows an example of two rotor angle time series; the black and red lines have acceptable and unacceptable rotor angle stability, respectively. Equation 2.15 defines the successive positive peak ratio, which uses the first and second positive peaks to quantify the damping of the generator.

$$SPPR = \frac{\text{Second Positive Peak} - \text{Minimum Value}}{\text{First Positive Peak} - \text{Minimum Value}} \leq 0.95 \quad (2.15)$$

In Figure 2.4, the first positive peak is denoted by a blue point, the second positive peak a green point, and the minimum value by a red point. The black line has $SPPR = 0.688$ which is considered to be a stable response.

The metrics discussed in this section will be used in this thesis to evaluate system stability after a perturbation. Specifically, I use a cascading failure simulation to evaluate system stability. Power system stability and cascading failures are highly interconnected phenomena; instabilities can precede cascades, or cascades can create instabilities. The next section

discusses the various ways cascading failures are modeled in the literature, and the model I use for this thesis work.

2.5 Cascading Failures in Power Systems

Cascading failures are a ubiquitous phenomenon in many different types of networks. Cascade models depend on the interaction of individual components and the topology of the network. When component interactions are linear, as in social networks, spreading occurs locally, among neighbors: when one component fails, the next component to fail will be one that is connected to the failed component. This is not the case in power systems, where cascades spread non-locally: when one component fails the next component failure is not necessarily adjacent. This is due to the non-linear nature of the system—something that cannot be modeled by linear approaches [22].

In power systems, cascading failures— colloquially named blackouts— refer to the sequential loss of transmission lines [21]. A cascade usually starts due to a random event, such as untrimmed vegetation falling on a line [13]. When a line fails, this causes the power flow to be redistributed among the remaining lines. Each transmission line has a maximum capacity of power it can transport; when this limit is exceeded, protection equipment stops the flow of current through the line. When power flow redistribution occurs, line flow limits might be exceeded, which causes another failure and necessitates further cutoffs and redistribution, thus continuing the cascade. While these dynamics are easy to describe, they are not easy to model. There are many approaches to modeling these cascades, some of which consider generator dynamics and some that do not.

A significant number of cascading failure models only implement the power flow equations outlined in Section 2.2. This is the simplest way to model cascades, while maintaining some sense of reality. The most prominent of these is the OPA model which is named after the

institutions of the authors [12]. OPA is run over many “days”, where each day the following occurs: (I) the initial power flow of the system is solved, using the DC approximation, (II) an initial set of lines are removed at the beginning of the day uniformly at random, (III) power flow is re-solved with these lines removed, (IV) remove any lines that become overloaded with some probability, (V) go back to (III) until no lines are overloaded. At the end of each “day” all lines that failed due to overload are upgraded, in that their capacity is increased, and the load that needs to be served is increased by some fraction.

The OPA model captures the important characteristics of models that do not include generator dynamics. It was used in an important study of self-organized criticality in power systems [8]. This study found that because a power system is operated in the most economical fashion (using all components at maximum capacity, when necessary), it is pushed toward a critical state where small perturbations can cause phase transitions (*i.e.* cascading failures) [4]. Specifically, the constant competition between providing more power generation and adding more capacity creates complexity in the power system dynamics. This has made the OPA model a popular choice for studies on other aspects of cascading failures [9, 19, 24].

Cascading failure models that consider generator dynamics—or transient stability—are less common in the literature, but they are important as larger amounts of VRG are added to power systems. Here, I discuss one cascading failure model that incorporates transient stability, but there are others [36, 52].

The model used for this thesis is a continuous phase space (CPS) model that was first presented by [11] and then adapted and modified in [63]. This model uses the DC power flow equations, as well as the generator swing equation 2.10 and load equation 2.11 for the transient dynamics. One distinguishing factor of the CPS model is the continuous nature of the line status. In most cascading failure models, the line status— η_{ij} —is a discrete variable. However, the CPS model treats it as a continuous variable and models it with a differential equation. Let c_{ij} represent the fractional line capacity being used, such that $c_{ij} = 1$ means

the line is at capacity. This capacity is defined by the maximum amount of charge that can flow through the line at any given time, or in other words, its maximum amount of energy. Thus, c_{ij} is equal to the integral of Equation 2.8a divided by the maximum amount of energy: $c_{ij} = \frac{B_{ij}(1-\cos\delta_{ij})}{W_{ij}}$.

In order to model the automatic removal of a line, the derivative of its status should become negative as $c_{ij} \geq 1$. Based on the CPS model of [63], the derivate is $\dot{\eta}_{ij} = f(\eta_{ij}) - c_{ij}$ where

$$f(\eta_{ij}) = \frac{1}{a} \left(\frac{1}{\eta_{ij}} - \frac{1}{1 - \eta_{ij}} \right) + a\eta_{ij}^4 - b$$

is a function that has three equilibria of $\dot{\eta}_{ij}$: stable ones at $\eta_{ij} < 1$ and $\eta_{ij} \approx 0$, and an unstable one at $\eta_{ij} \approx 1$. In practice, $f(\eta_{ij})$ could be any function with the desired equilibria. [11] uses a sum of exponentials. But I will remain consistent with [63] for this work. The necessary equations for the CPF model are given by Equations 2.16.

$$\dot{\eta}_{ij} = 10(f(\eta_{ij}) - \frac{B_{ij}(1 - \cos\delta_{ij})}{W_{ij}}) \quad \forall i, j \in E \quad (2.16a)$$

$$\dot{\omega}_g = -\frac{D_g}{M_g}\omega_g - \frac{1}{M_g}(P_g + \sum_{\forall i \notin G} B_{gi} \sin \delta_{gi}) \quad \forall g \in G \quad (2.16b)$$

$$\dot{\delta}_g = \omega_g - \omega_1 \quad \forall g \in G \quad (2.16c)$$

$$\dot{\delta}_i = -\frac{1}{D_i}(P_i + \sum_{j=1}^{n_b} B_{ij}\eta_{ij} \sin \delta_{ij}) - \omega_1 \quad \forall i \notin G \quad (2.16d)$$

The CPS model as defined in [63] does not consider renewable generation sources, which is an essential component of this thesis work. Similar to the approach taken in [58], the generator equations in the CPS model can be modified by setting $M_g = 0$. This change is shown in Equation 2.17, which has a similar form to the load equation (2.11).

$$\dot{\delta}_{RG} = -\frac{1}{D_{RG}}(P_{RG} + \sum_{\forall i \notin G} B_{RG,i} \sin \delta_{RG,i}) - \omega_1 \quad (2.17)$$

Equation 2.17 is essentially like modeling a renewable source connected to a droop controller inverter, which is the simplest control mechanism in use [51]. This equation does not, however, model the temporal power output of the generator P_{RG} because the time scales considered here are small enough to model it as a constant [28].

My thesis work considers the importance of inertia in power system stability. The mathematical relevance of inertia was discussed in Section 2.3.1. I will expand further on the dynamical importance of inertia in the next chapter. Section 2.4.1 defined the metrics I will use to evaluate system stability, with a focus on frequency and rotor angle stability. Finally, Section 2.5 introduced cascading failures as one type of power system perturbation, as well as the cascading failure model I will use for my thesis work. The next chapter lays out the proposed work and preliminary results in more detail.

Chapter 3

Role of Power System Inertia in Cascade Events

Power systems with high proportions of variable renewable generation (VRG), and therefore less inertia, have experienced increasing issues with stability and resiliency during cascades. For example, in 2016 a large blackout occurred in Australia where the entire southern region lost power. Preceding the blackout, wind generation was providing almost 50% of the power in that region when tornadoes disconnected multiple transmission lines. As a result, the interconnection lines between the north and the south overloaded and were tripped. The southern system did not have enough traditional synchronous generation (SG) available to stabilize the inevitable frequency deviations, which resulted in a frequency collapse [43].

The Southern Australia blackout underscores the need to understand the function of inertia during cascading failures. Specifically, two key aspects of inertia contributed to the blackout. First, high levels of renewable generation in the south meant low *total system inertia*. Second, the large-inertia SG (coal, natural gas) was easily separated from the low-inertia (wind); only a few transmission lines had to fail for the low-inertia generation to become isolated from the large-inertia generation. I will describe this issue as the *structural distribution of inertia*.

Both of these aspects of inertia—the overall amount and its location on the network—are crucial to system stability during cascading failures. The goal of this thesis is to gain a deeper understanding of the role of inertia in power system stability with a specific focus on the cascading failure dynamics of synthetic power systems.

Total system inertia has only been addressed by a few studies in limited contexts. Several investigations explored the effect of lower system inertia on system stability [16, 33, 34, 62], but exhaustive research on the relationship between system stability and total system inertia is notably absent from the literature. There is a documented need for this type of study; this past year, for instance, the Australian Energy Market Operator (AEMO) started requiring all power system operators to determine the level of system inertia needed to maintain system stability.

To address this gap, I will conduct an experiment that decreases total system inertia uniformly across the network—*i.e.*, reducing the inertia constant of every generator¹. The goal here is to study a simplified version of the problem that neglects the spatial distribution of inertia on the nodes of the network. This will allow for general conclusions to be drawn about the relationship between *total* system inertia and system stability.

The experiment proposed in the previous paragraph is not completely realistic, however; a better representation decreases inertia in a neighborhood of the network. This issue has only recently been recognized as a concern in the power-systems community [33]. Many studies about inertia placement in these systems have used unrealistically small test cases [55, 59]. Larger studies only focused on placement of control mechanisms, or only explored a few possible low-inertia scenarios [46, 62]. A study of a wide range of inertia distribution scenarios is needed because renewable generation is not added uniformly across the network. This is due to both resource availability and political incentives. The types of problems

¹Recall from Section 2.3, that total system inertia is the weighted sum of the inertia provided by every generator in the system (Equation 2.13)

that can arise from a poor placement of inertia are exemplified in the Southern Australian blackout.

The second part of the proposed work will explore this aspect of inertia. I will perform a wide range of possible inertia placement scenarios. Inertia values will be chosen based on representative values for given generation types (see Table 2.1). For this part of the study, I am specifically interested in how the separation between low and high inertia impacts stability. One way to quantify “separation” is by the average path length between generators with large and small inertia. I hypothesize that as the average path length between large and small inertia generation units increases, system instabilities during cascades will also increase. My placement scenarios will be chosen to explore this.

3.1 Experimental Setup

U.S. power grids are considered to be critical infrastructure. This means that information about the system—such as its structure and parameters—is exempt from public release. Therefore, it has become standard practice in the power systems community to experiment with synthetic networks that match the topology and dynamics of a power system *statistically*.

Following that approach, I will conduct the two proposed inertia alterations introduced above on two synthetic power network test cases. The first synthetic network is constructed using population and generation statistics for central Illinois with 200 nodes, 49 of which are generators; the second is based on the South Carolina power system with 500 nodes, 90 of which are generators. I will refer to these as the Illinois 200 bus test case and the South Carolina 500 bus test case, respectively. Both of these test cases are shown in Figure 3.1, with generators in green and all other buses in red.

Neither of these cases contain specific information about the actual power systems they

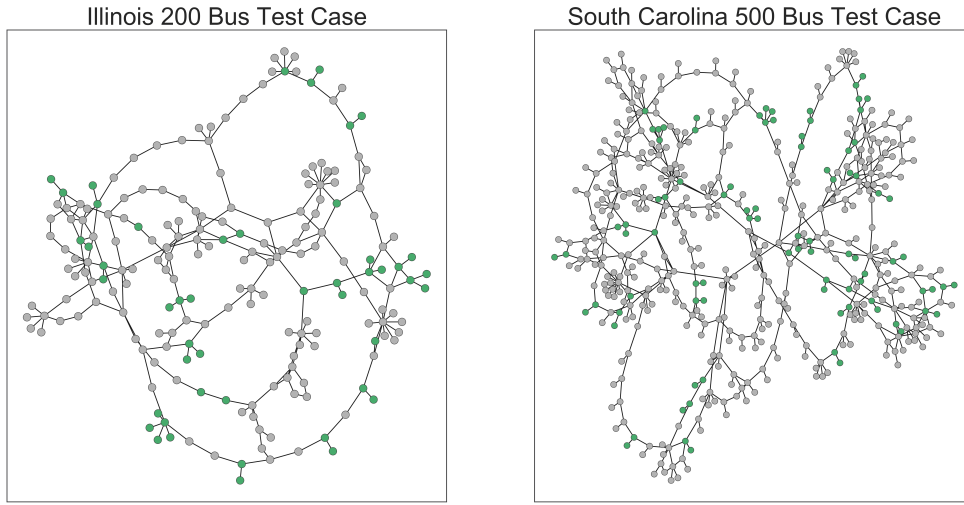


Figure 3.1: Plot of the power system test cases for the proposed experiments. Generators are marked in green; all other buses are in red.

represent. Rather, they were created using known information about the respective regions. Recall from Section 2.2, a basic requirement for any power systems study is the specification of the load and generation. For these test cases, the load information is based on the population data of that region and the generation type and size is based on data from the Energy Information Administration [6, 29]. Data about the generator dynamics, such as the inertia constants, are drawn from a distribution created from well-established test cases [61]. Finally, [60] applied a tuning procedure to the governor and stabilizer controls using common algorithms. The tuning was guided by standard stability metrics, some of which are outlined in Section 2.4.1.

For the purposes of this work, I made a few alterations to these test cases. First, [61] treat wind generators as having inertia. For realism, I will model all wind generators with no inertia. Second, solar generators are “netted” with the load. This means that the modeled power consumption is decreased by the total solar generation and the dynamics of these generators are not modeled. In this work, solar generator dynamics are modeled explicitly,

in a similar fashion as wind generators.

To study the effects of inertia on stability, I will run transmission line cascading failure simulations for the two sets of experiments listed above. Each cascade simulation generates a time series of the real power flow on each line, the voltage angle of every bus, and the rotor speed and angle of every generator. The specific cascading failure model is described in Section 2.5. Each simulation will be conducted in the following way. First, all parameters, including any inertia values, are initialized using data from [61] and the MATPOWER package [64]; then Equations 2.16 are solved using the Matlab `ode15s` solver for a time period of 20 seconds to ensure the system reaches a steady-state. (A time period of 20 seconds is approximately the amount of time that passes before generator control mechanisms turn on [49].) This will produce the baseline values for the system. Then I will trip k line(s) and re-run the simulation.

To quantify the severity of each cascade simulation, I will use a number of metrics on the total system frequency time series. Recall that the equation for total system frequency is a weighted average of the frequency of every generator (see Section 2.4). The two metrics of interest on the total system frequency time series are the maximum frequency deviation and the rate of change of frequency (RoCoF); both of these metrics are concerns as system inertia changes [33].

3.2 Preliminary Results

This section presents the results from the first experiment (reducing total system inertia) on the Illinois 200 bus test case. I refer to the scenario where no inertia changes are made as the “base total inertia”, or M_{tot} . Each change in total system inertia is given as a fraction or percentage of M_{tot} . The results of each cascade simulation are grouped into four categories according to the outcome of the simulation, as shown in Figure 3.2. Category (I) consists

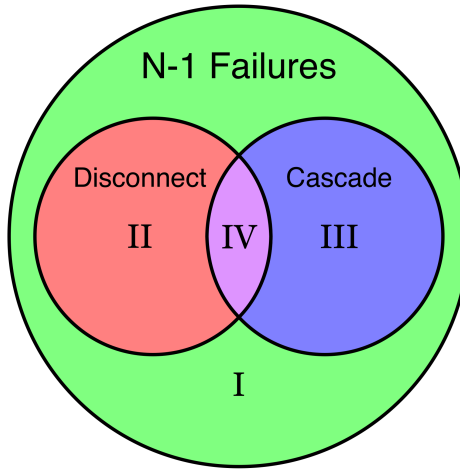


Figure 3.2: Set of outcomes that can occur after an initial failure. (I) No other failures occur and the network remains connected. (II) $N - 1$ contingency disconnects the network, but no other failures occur. (III) A cascade of failures occurs but the network remains connected. (IV) A cascade of failures occurs and the network disconnects. The sizes of the circles do not indicate the number of scenarios that belong in each category.

of the set of line contingencies that do not disconnect the network and do not result in a cascade. This is the largest category for the Illinois 200 bus system; of the 245 possible line failures, 171 of them fall into this category. Although this group of contingencies represents a class of failures with relatively stable dynamics, those dynamics are still important to understand. For instance, the European Network of Transmission System Operators for Electricity (ENTSO-E) have indicated a need to quantify the RoCoF limits of system devices in terms of “normative” contingencies and future changes in system inertia [17]. Category (I) contingencies can be considered “normative” because the system returns to a steady-state without any other failures. Therefore, system limits should encompass all possible dynamics of category (I) contingencies, which requires a deeper understanding of those dynamics.

An example of the dynamical response to inertia changes for category (I) contingencies for the Illinois 200 bus test case is shown in Figure 3.3. Most prominently, as total inertia decreases the maximum frequency deviation increases. At the base total inertia the maximum

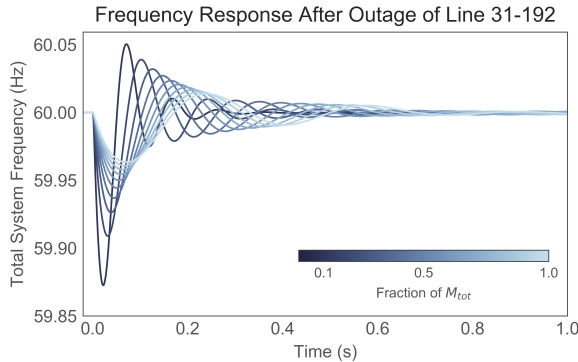


Figure 3.3: Frequency dynamics of the Illinois 200 bus test case for an outage that falls into category (I).

frequency deviation is approximately 0.01 Hz; this deviation increases to 0.2 Hz at 10% the base total inertia. Furthermore, the maximum deviation occurs at an earlier time as inertia decreases, which indicates an increasing RoCoF. Although a 90% reduction in inertia is not happening in the near future, it is informative to understand how the maximum frequency and RoCoF change as total system inertia decreases. To that end, Figures 3.4a and 3.4b show the maximum frequency deviation and RoCoF averaged over all category (I) contingencies. Clearly, both of these measures have a non-linear relationship with inertia. For each measure, I tried fitting different functions—exponentials, power law, *etc.*—to the data. The best fit, shown in blue, is of the form $a * x^{-b}$ for both measures². The average maximum frequency deviation seems to scale as $\approx 1/M_{tot}^{0.12}$ and the RoCoF $\approx 1/M_{tot}^{0.79}$. This preliminary result quantifies the overall general trend of frequency and total system inertia. Other studies have generally found linear, rather than power-law, trends perhaps because they have only explored a limited number of inertia values [62].

Of course, the averages shown in Figures 3.5a-3.5b are influenced by contingencies that cause larger deviations. Figure 3.5a shows the frequency deviation for each category (I) contingency. For clarity, contingencies with a larger value are shown with a darker color.

²To verify this fit, I took the logarithm of the total system inertia and each frequency measure and again solved for the best fit. Both fits are linear, the slope for the maximum frequency deviation is -0.1168 with $R^2 = 0.9986$ and the slope for the RoCoF is -0.876 with $R^2 = 0.9982$.

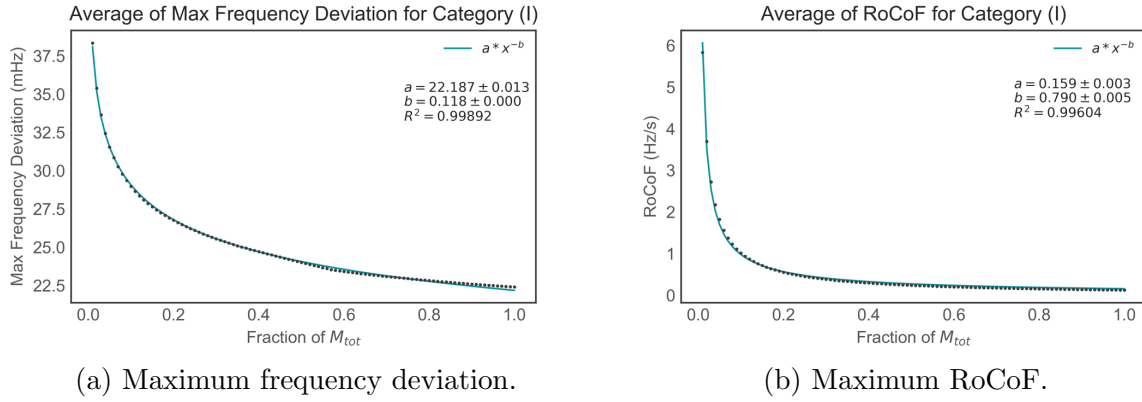


Figure 3.4: Average over all category (I) contingencies of the maximum RoCoF for the Illinois 200 bus test case.

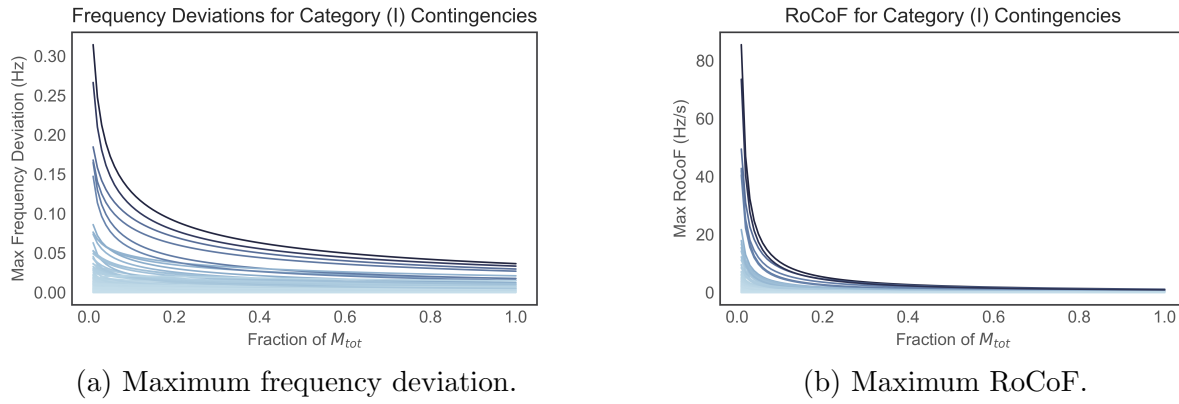


Figure 3.5: Frequency dynamics for each category (I) contingency as a function of inertia for the Illinois 200 bus test case. For clarity, a darker line color indicates a larger magnitude.

Indeed, not all contingencies appear to grow in the same manner as the average shown in Figure 3.4a. For example, the contingency shown in Figure 3.3 is the darkest line in Figure 3.5a, and has nonlinear growth. However, it is also clear that if no deviation occurs at the base total system inertia, a decrease in inertia does not cause a deviation to occur (*i.e.* inertia is only important when a deviation occurs). Similarly, the RoCoF of each contingency is plotted in Figure 3.5b. The growth in RoCoF is more dramatic at low inertia values than the maximum frequency deviation. This makes sense because inertia specifically deals with a *change* in motion; less inertia means it is easier to move things faster.

So far, all of these results have only investigated how the frequency dynamics change with

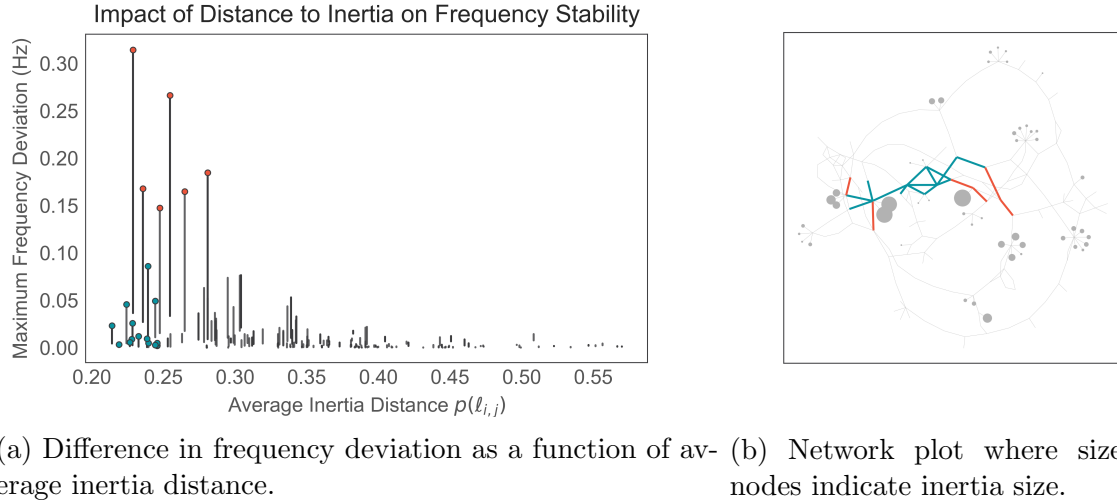


Figure 3.6: Impact of inertia distance on frequency deviations for category (I) contingencies of the Illinois network. The colored points in the left plot correspond to the colored edges in the right plot.

total system inertia. As seen in Figures 3.5a and 3.5b, there is a wide range of possible frequency dynamics. This is likely due to the structure of the network, specifically the location of the contingency in relation to the generators. To better understand this, I introduce a new measure called the *average inertia distance* that quantifies the distance of a contingency to the inertia in the system, given by Equation 3.1. asdf

$$p(\ell_{i,j}) = \frac{1}{M_{tot}} \sum_{g=1}^{n_g} M_g \frac{d(\ell_{i,j}, g)}{\text{diam}(G)} \quad (3.1)$$

Explicitly, let i and j be the buses that are connected by line $\ell_{i,j}$, the initially tripped line. I compute the minimum path length of each bus to a generator g and assign the minimum as the distance between the line and the generator $d(\ell_{i,j}, g) = \min[d(i, g), d(j, g)]$. I scale $d(\ell_{i,j}, g)$ by the longest shortest path in the network—the diameter of the network— $\text{diam}(G)$. I assign the weight $\frac{M_g}{M_{tot}}$ inertia to this distance.

Figure 3.6 shows the relationship between the average inertia distance and maximum frequency deviations. Figure 3.6a plots the change in the maximum frequency deviation from M_{tot} to $0.01M_{tot}$ for each contingency as a function of the average inertia distance. The

length of the line indicates the change in the maximum frequency deviation, and the horizontal location indicates the average inertia distance. Figure 3.6b plots the Illinois network with the size of the nodes indicating the amount of inertia provided by that node (generators with $M_g = 0$ have a small size to distinguish them from non-generator nodes). The colored edges in Figure 3.6b correspond to the colored point in Figure 3.6a. In general, as the average inertia distance increases (*i.e.* contingencies are closer to larger-inertia generators), the maximum frequency deviation increases. For example, the red points in Figure 3.6a are indeed close to large inertia generation in Figure 3.6b. Most of them are only one link away from the large-inertia generation. However, there are some notable exceptions, marked with a blue point in Figure 3.6a and a blue edge in Figure 3.6b. First, these contingencies have as high or higher average inertia distance to the red points, but have a much lower frequency deviation. Based on Figure 3.6b the blue contingencies are not just close to one cluster of large inertia generation but are close to *multiple* large-inertia generation sources. This might suggest that frequency deviations from multiple generation sources are cancelling each other out, reminiscent of an interference pattern.

The previous paragraph suggests two conjectures. First, the distance to large-inertia generation is a general framework for determining the size of a frequency deviation. Specifically, the farther away a contingency occurs from large-inertia generation sources, the less impact it has on system frequency. Second, the closer to large-inertia sources, the more the network *topology* matters. Indeed, the blue edges in Figure 3.6b are part of triangles and cycles. They appear to be the “spine” of the network.

A less dynamically stable outcome of a line contingency is one that results in a cascade, but does not disconnect the network: category (III) in Figure 3.2. The Illinois 200 bus test case only has one contingency that falls into this category. Figure 3.7a plots the time series for this contingency for various values of total system inertia and Figure 3.7b-3.7c show the frequency dynamics. The frequency dynamics follow a pattern similar to category (I)

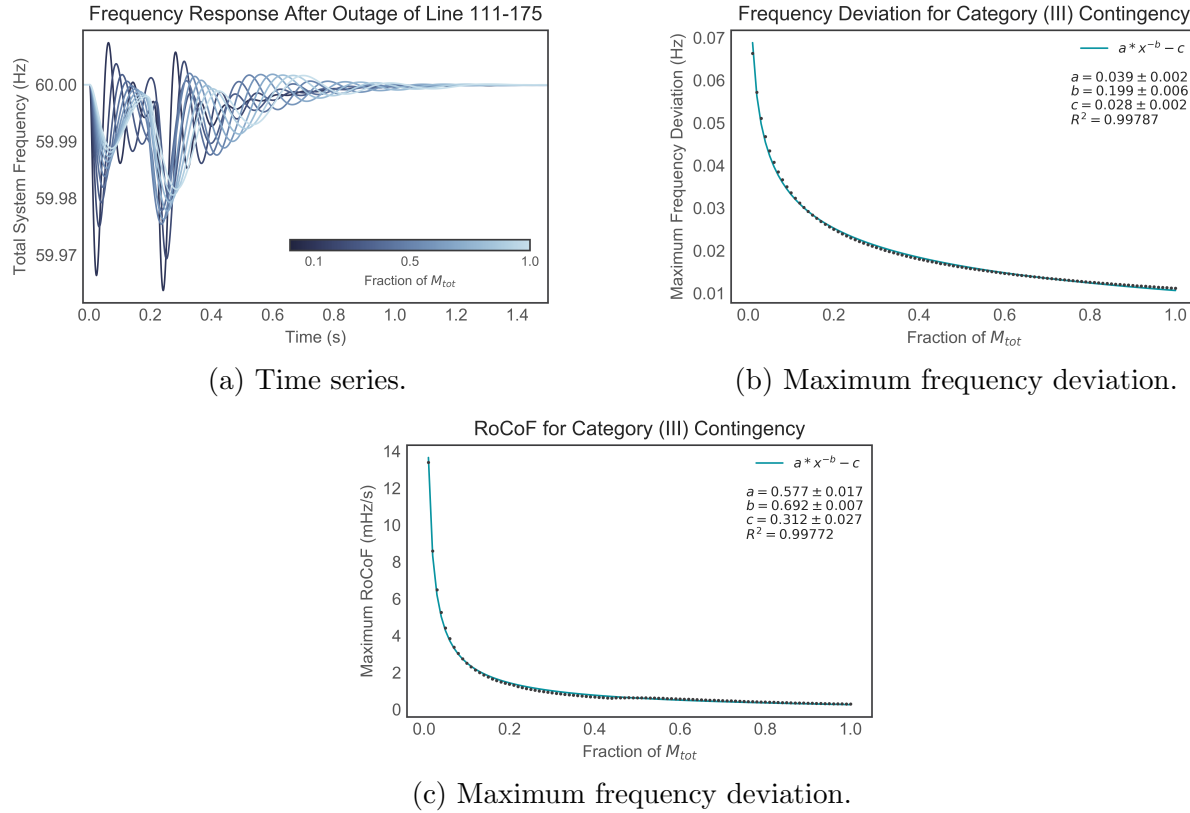


Figure 3.7: Frequency dynamics for the category (III)

contingencies. This is because the network remains connected in this case, which means that the coupling between all of the dynamic components does not change dramatically. As such, categories (I) and (III) can be considered dynamically similar.

Finally, the last two categories can be considered the least dynamically stable as they result in a disconnected network. There are two ways this can happen: either the original contingency disconnected the network or the original contingency caused a cascade that split the network. These are categories (II) and (IV) in Figure 3.2, respectively.

There are two types of category (II) contingencies (because there are only two bus types in the model): one that disconnects a load bus, and one that disconnects a generator. The former is usually studied as a remedial action, while the latter is often studied as an initiating event. Recall from Section 2.4 that frequency and rotor angle stability involve the study of

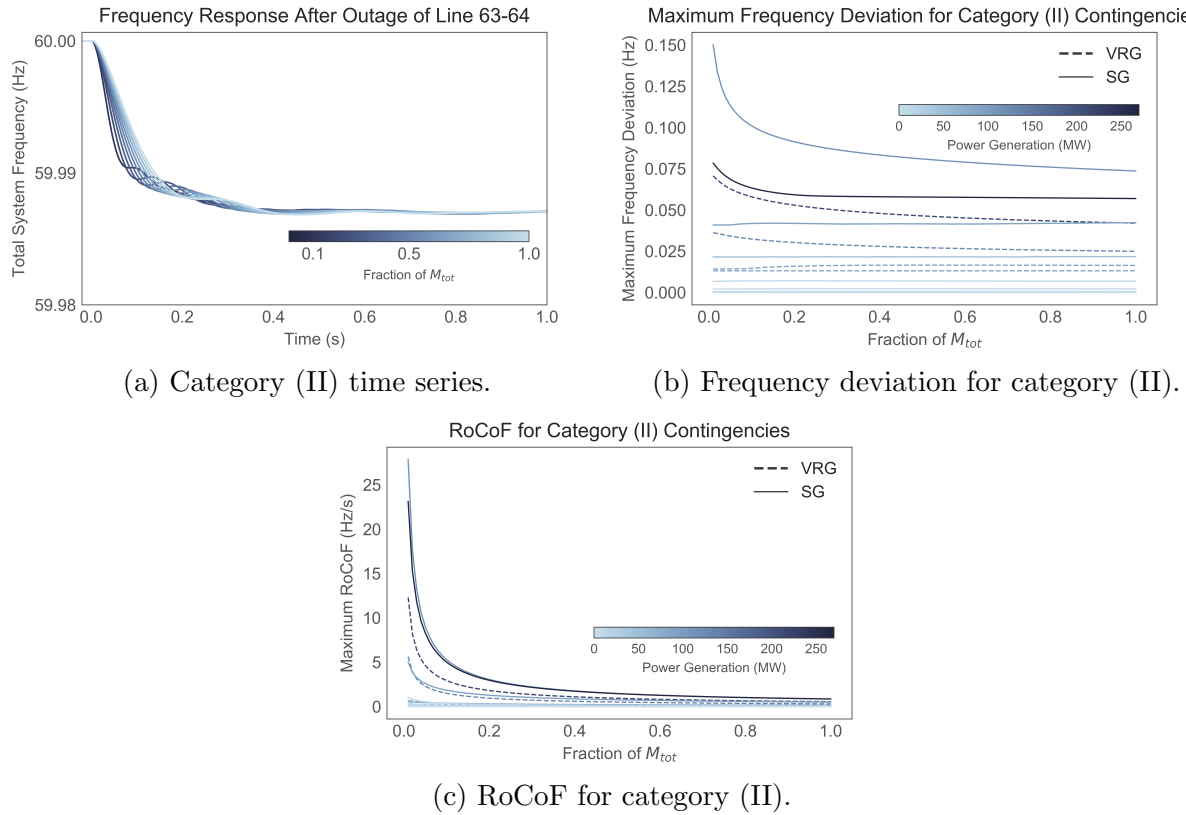


Figure 3.8: Category (II) time series and frequency dynamics for the Illinois test case.

system dynamics after the loss of generation or load (although these instabilities can occur for line losses as well). Here, I focus on generators, as is the convention in the literature. Recall from earlier in this chapter that the Illinois test case already incorporates VRG. The removal of different types of generation sources induces different dynamics. For example, Figure 3.8a shows the frequency time series at various inertia values after the removal of VRG at bus 64. Similar to the other categories, the final settling frequency is consistent for all inertia values. Additionally, the RoCoF seems to increase as total system inertia decreases, as shown in Figure 3.8c. However, the first valley of the time series occurs at a lower frequency for higher values of total system inertia. This is the opposite behavior from categories (I) and (III) (and category (IV) as discussed in a moment). Based on Figure 3.8b, there are even some contingencies that have a slight decrease in frequency deviation as system inertia decreases. One possible reason for this is the amount of power the generators

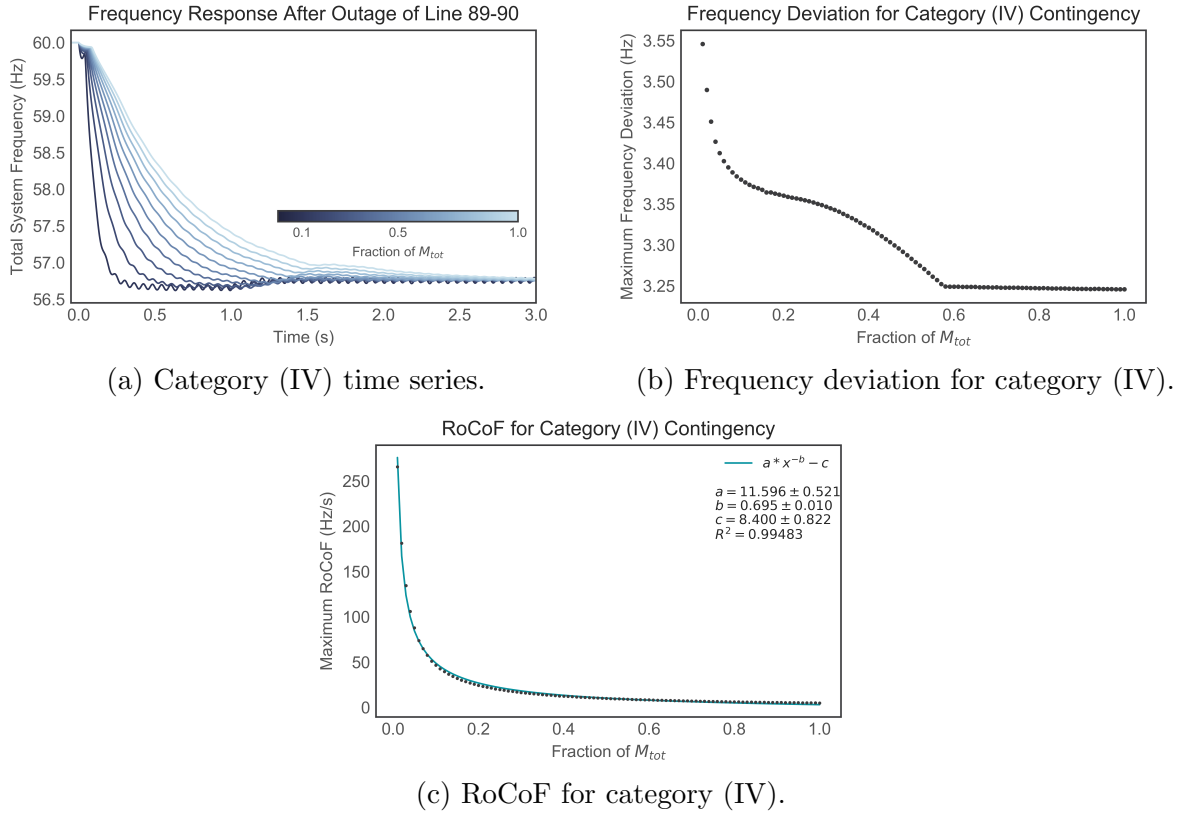


Figure 3.9: Category (IV) time series and frequency dynamics for the Illinois test case.

are providing. Larger power providers, regardless of whether it that power is SG or VRG, have a functional form similar to categories (I) and (III). This would explain the difference in the two contingencies that start at the same deviation at the base total system inertia, and then deviate. The second reason this could be occurring is illustrated by category (IV), described below.

Figure 3.9 shows the dynamics for the only category (IV) contingency of the Illinois test case. The time series has a similar step-like behavior as the results shown in Figure 3.8a for category (II), but it also has increased oscillatory behavior as inertia decreases, as in category (III). The RoCoF behavior is consistent with all other categories. However, the maximum frequency deviation has more complicated behavior. The deviation hardly changes from the base total inertia to approximately $0.6M_{tot}$. Then, the maximum frequency deviation increases, but with inverted concavity as compared to the other categories. Finally, at

about $0.2M_{tot}$, the growth trend appears to match that of other categories. Looking closely at Figure 3.9a, one can see a small peak at approximately 1.5 seconds that slightly grows in magnitude as inertia decreases. This peak is what causes the first change in behavior at $0.6M_{tot}$. Specifically, $0.6M_{tot}$ is the inertia value that this oscillation has a lower amplitude than the final settling frequency. As total system inertia continues to decrease, smaller oscillations start to grow. The concavity transition at $0.2M_{tot}$ is the point at which the amplitude of the small oscillatory behavior becomes larger than the fixed point value of ≈ 56.75 Hz. Concretely, the idealized flat frequency behavior after a loss of generation shown in Figure 2.3 will be less and less realistic as total system inertia decreases [33]. The results shown in Figure 3.9 possibly indicate one way of determining when the fixed point attractor bifurcates to a limit cycle oscillator.

To review my results: I divided the cascading failure dynamics into four categories based on their outcomes. I then analyzed their trends from most stable to least with the following findings. First, although experiment one artificially changed total system inertia, it is incorrect to assume that the change in frequency deviation and RoCoF has a linear relationship with total system inertia. Second, the size of a frequency deviation depends on the network structure. In general, the frequency deviation size increases when a contingency is closer to large-inertia generation. However, even this has caveats: the substructure that the contingency is a part of probably determines its effects on stability. Finally, categories (II) and (IV) showed oscillatory behavior around the final frequency value that increased as total system inertia decreases. This indicates that limit cycle behavior will be amplified as inertia decreases, increasing the risk of generation loss. These preliminary results are a promising start to understanding the role of inertia in power system stability. The work remaining to complete that investigation is described in the following chapter.

Chapter 4

Conclusion

My overall thesis work addresses the role of inertia in power system stability. I divide this issue into two parts: the *total* system inertia and the *structural distribution* of inertia. The preliminary results presented in Chapter 3 addressed the first of those two parts: the relationship between total system inertia and power system dynamics. Specifically, I showed that the frequency dynamics have a nonlinear dependence on total system inertia. Previously work had revealed a linear relationship by only using a limited range of inertia values [34][62]. My broader finding of a non-linear relationship could have important implications for policy makers that will decide how to change frequency limits of power system devices, which in turn impacts grid resiliency [17]. My preliminary results also addressed the second part of my overall thesis questions: network topology is a crucial aspect of frequency stability. Specifically, I defined a new metric called the *average inertia distance* that calculates the distance between a contingency and inertia providing generation. The average inertia distance generally captures the relationship between contingency location and the frequency dynamics. I showed that there is still nuance in this metric; even contingencies with low average inertia distance can have low frequency deviation. The total system inertia experiment has been completed for the Illinois test case, and will be completed for the South Carolina test

case within the next month.

The rest of my thesis work will be devoted to a more-detailed study of the impact of the structural distribution of inertia on system stability. Although the impact of system topology was revealed by the experiment on total system inertia, this is only one specific case and requires further investigation. Among other things, this will require the development of other measures that can capture the relationship between the system dynamics and network structure. Two measures used in the literature are motif analysis and basin stability. Motif analysis analyzes the subgraphs of a network in order to find structures that are relevant to the dynamics of the network. It has been largely applied to biological networks, but could be used to understand the structural significance of the blue edges in Figure 3.6b [35]. On the other hand, *basin stability* is a measure of the basin of attraction of a dynamical system. This method uses a Monte Carlo algorithm to randomly perturb state variables and then counts the number of times the system returns back to the original equilibrium [32]. The basin stability approach has also been used to analyze power system models in conjunction with motif analysis but has never been used to explore the effects of inertia on stability [31][50].

The timeline for the remaining work is the following: March 2019-May 2019 will be devoted to finalizing the total system inertia exploration for both test cases and preparing the results for journal submission. During June 2019-August 2019 I will define inertia distributions that more carefully probe the effects of network topology and system dynamics. Additionally, during this time period I will run the cascading failure simulations as described in Section 3.1. During the period of August 2019-December 2019 I will analyze the results using similar metrics from the first experiment, along with the measures mentioned above. Finally, I will write up my results during the time period of December 2019 - March 2020 to submit to journals. After this, I will write my dissertation with a planned graduation date of December 2020.

Bibliography

- [1] S. Abe, Y. Fukunaga, A. Isono, and B. Kondo. Power system voltage stability. *IEEE Transactions on Power Apparatus and Systems*, PAS-101(10):3830–3840, 1982.
- [2] Energy Information Administration. Annual energy outlook 2018. Technical report, 2-6-2018.
- [3] A. Arenas, A. Daz-Guilera, J. Kurths, Y. Moreno, and C. Zhou. Synchronization in complex networks. *Physics Reports*, 469(3):93 – 153, 2008.
- [4] P. Bak. Self-organized criticality. *Physica A*, 163(1):403 – 409, 1990.
- [5] D. Bienstock. *Electrical Transmission System Cascades and Vulnerability: An Operations Research Viewpoint*. MOS-SIAM Series on Optimization, New York, NY, USA, 2015.
- [6] A. B. Birchfield, Ti Xu, K. M. Gegner, K. S. Shetye, and T. J. Overbye. Grid structural characteristics as validation criteria for synthetic networks. *IEEE Transactions on Power Systems*, 32(4):3258–3265, jul 2017.
- [7] M. B. Cain, R. P. O'Neill, and A. Castillo. History of optimal power flow and formulations, paper 1. Technical report, FERC, 2012.
- [8] B. A. Carreras, V. E. Lynch, I. Dobson, and D. E. Newman. Complex dynamics of blackouts in power transmission systems. *Chaos*, 14(3):643–652, 2004.

- [9] J. Chen, J. S. Thorp, and I. Dobson. Cascading dynamics and mitigation assessment in power system disturbances via a hidden failure model. *International Journal of Electrical Power and Energy Systems*, 27(4):318 – 326, 2005.
- [10] Congress. Energy policy act of 2005. *Pub.L. 109-58*, 2005.
- [11] C. L. DeMarco. A phase transition model for cascading network failure. *IEEE Control Systems*, 21(6):40–51, Dec 2001.
- [12] I. Dobson, B. A. Carreras, V. E. Lynch, and D. E. Newman. An initial model for complex dynamics in electric power system blackouts. In *Proceedings of the 34th Annual Hawaii International Conference on System Sciences*, pages 710–718, 2001.
- [13] V. Donde, V. Lopez, B. Lesieutre, A. Pinar, C. Yang, and J. Meza. Identification of severe multiple contingencies in electric power networks. In *Proceedings of the 37th Annual North American Power Symposium, 2005.*, pages 59–66, 2005.
- [14] F. Dörfler and F. Bullo. Synchronization and transient stability in power networks and nonuniform kuramoto oscillators. *SIAM J. Control Optim.*, 50(3):1616–1642.
- [15] F. Dörfler and F. Bullo. Kron reduction of graphs with applications to electrical networks. *IEEE Transactions on Circuits and Systems I: Regular Papers*, 60(1):150–163, Jan 2013.
- [16] S. Eftekharnejad, V. Vittal, G. T. Heydt, B. Keel, and J. Loehr. Impact of increased penetration of photovoltaic generation on power systems. *IEEE Transactions on Power Systems*, 28(2):893–901, 2013.
- [17] ENTSO-E. Rate of change of frequency (rocof) withstand capability, Mar. 2017.
- [18] EPA. Sources of greenhouse gas emissions, 2016. <https://www.epa.gov/ghgemissions/sources-greenhouse-gas-emissions> [Accessed: 8-27-2018].

- [19] M. J. Eppstein and P. D. Hines. A random chemistry algorithm for identifying collections of multiple contingencies that initiate cascading failure. *IEEE Transactions on Power Systems*, 27(3):1698–1705, 2012.
- [20] ERCOT. Inertia: Basic concepts and impacts on the ERCOT grid, Apr 2018.
- [21] R. Baldick et. al. Initial review of methods for cascading failure analysis in electric power transmission systems. In *2008 IEEE Power and Energy Society General Meeting - Conversion and Delivery of Electrical Energy in the 21st Century*, pages 1–8, 2008.
- [22] R. Fitzmaurice, E. Cotilla-Sanchez, and P. D. Hines. Evaluating the impact of modeling assumptions for cascading failure simulation. In *Power and Energy Society General Meeting, 2012 IEEE*, pages 1–8. IEEE, 2012.
- [23] D. J. Griffiths. *Introduction to Electrodynamics*. Pearson Education, Inc., 4th edition, 2013.
- [24] P. D. Hines, I. Dobson, E. Cotilla-Sanchez, and M. Eppstein. “Dual Graph” and “Random Chemistry” methods for cascading failure analysis. In *2013 46th Hawaii International Conference on System Sciences*, pages 2141–2150, 2013.
- [25] P. Kundur, J. Paserba, V. Ajjarapu, G. Andersson, A. Bose, C. Canizares, N. Hatziargyriou, D. Hill, A. Stankovic, C. Taylor, T. Van Cutsem, and V. Vittal. Definition and classification of power system stability ieee/cigre joint task force on stability terms and definitions. *IEEE Transactions on Power Systems*, 19(3):1387–1401, 2004.
- [26] P. S. Kundur. *Power System Stability and Control*, pages 1–12. CRC Press, 2012.
- [27] H. G. Kwatny and K. Miu-Miller. *Power System Dynamics and Control*. B. Basel, 2016.
- [28] M. Lave and J. Kleissl. Solar variability of four sites across the state of colorado. *Renewable Energy*, 35(12):2867–2873, 2010.

- [29] H. Li, A. L. Bornsheuer, T. Xu, A. B. Birchfield, and T. J. Overbye. Load modeling in synthetic electric grids. In *2018 IEEE Texas Power and Energy Conference (TPEC)*, pages 1–6, Feb 2018.
- [30] J. Machowski, J. W. Bialek, and J. R. Bumby. *Power system dynamics: stability and control*. Wiley, second edition, 2008.
- [31] P. J. Menck, J. Heitzig, J. Kurths, and J. H. Schellnhuber. How dead ends undermine power grid stability. *Nature communications*, 5:3969, 2014.
- [32] P. J. Menck, J. Heitzig, N. Marwan, and J. Kurths. How basin stability complements the linear-stability paradigm. *Nature physics*, 9(2):89, 2013.
- [33] F. Milano, F. Dörfler, G. Hug, D. Hill, and G. Verbic. Foundations and challenges of low-inertia systems. In *Power Systems Computation Conference (PSCC)*, Dublin, Ireland, 2018. To appear.
- [34] N. W. Miller, M. Shao, S. Pajic, and R. D'aquila. Western wind and solar integration study phase 3 frequency response and transient stability. Technical report, National Renewable Energy Lab, Golden, CO, 2014.
- [35] R. Milo, S. Shen-Orr, S. Itzkovitz, N. Kashtan, D. Chklovskii, and U. Alon. Network motifs: simple building blocks of complex networks. *Science*, 298(5594):824–827, 2002.
- [36] D. P. Nedic, I. Dobson, D. S. Kirschen, B. A. Carreras, and V. E. Lynch. Criticality in a cascading failure blackout model. *International Journal of Electrical Power & Energy Systems*, 28(9):627 – 633, 2006.
- [37] NERC. A technical reference paper fault-induced delayed voltage recovery. 2009.
- [38] NERC. 2018 frequency response annual analysis, Nov. 2018.
- [39] NERC. About nerc. <http://www.nerc.com/AboutNERC/Pages/default.aspx>, 7-11-2017.

- [40] NERC. Interconnections. <http://www.nerc.com/AboutNERC/keyplayers>, 7-11-2017.
- [41] T. Nishikawa and A. E. Motter. Comparative analysis of existing models for power-grid synchronization related content improving power grid transient stability by plug-in electric vehicles. *New Journal of Physics*, 17, 2015.
- [42] Electric Reliability Council of Texas. 2017 state of the grid, Apr 2018.
- [43] Australian Energy Market Operator. Black system south australia 28 september 2016 - final report, 2017.
- [44] T. J. Overbye, X. Cheng, and Y. Sun. A comparison of the ac and dc power flow models for lmp calculations. In *System Sciences, 2004. Proceedings of the 37th Annual Hawaii International Conference on*. IEEE, 2004.
- [45] Southwest Power Pool. Southwest power pool disturbance performance requirements, Jul 2016.
- [46] B. K. Poolla, S. Bolognani, and F. Dörfler. Optimal placement of virtual inertia in power grids. *IEEE Transactions on Automatic Control*, 62(12):6209–6220, December 2017.
- [47] K. Purchala, L. Meeus, D. Van Dommelen, and R. Belmans. Usefulness of dc power flow for active power flow analysis. In *Power Engineering Society General Meeting, 2005. IEEE*, pages 454–459. IEEE, 2005.
- [48] C. Roberts. Review of international grid codes, Feb 2018.
- [49] P. W. Sauer and M. A. Pai. Power system dynamics and stability. *Urbana*, 1998.
- [50] P. Schultz, J. Heitzig, and J. Kurths. Detours around basin stability in power networks. *New Journal of Physics*, 16(12):125001, 2014.

- [51] J. W. Simpson-Porco, F. Dörfler, and F. Bullo. Droop-controlled inverters are kuramoto oscillators. *IFAC Proceedings Volumes*, 45(26):264–269, 2012.
- [52] J. Song, E. Cotilla-Sánchez, G. Ghanavati, and P. D. Hines. Dynamic modeling of cascading failure in power systems. *IEEE Transactions on Power Systems*, 31(3):2085–2095, 2016.
- [53] B. Stott, J. Jardim, and O. Alsaç. Dc power flow revisited. *IEEE Transactions on Power Systems*, 24(3):1290–1300, 2009.
- [54] J. Sun. Impedance-based stability criterion for grid-connected inverters. *IEEE Transactions on Power Electronics*, 26(11):3075–3078, 2011.
- [55] A. Ulbig, T. S. Borsche, and G. Andersson. Impact of low rotational inertia on power system stability and operation. *IFAC Proceedings Volumes*, 47:7290–7297, 2014.
- [56] J. Undrill. Primary frequency response and control of power system frequency, Feb. 2018.
- [57] A. Von Meier. *Electric power systems: a conceptual introduction*. John Wiley & Sons, 2006.
- [58] C. Wang, C. Grebogi, and M. S. Baptista. Control and prediction for blackouts caused by frequency collapse in smart grids. *Chaos: An Interdisciplinary Journal of Nonlinear Science*, 26(9):093119, 2016.
- [59] Y. Wang, H. Silva-Saravia, and H. Pulgar-Painemal. Estimating inertia distribution to enhance power system dynamics. pages 1–6, 2017.
- [60] T. Xu, A. B. Birchfield, and T. J. Overbye. Modeling, tuning, and validating system dynamics in synthetic electric grids. *IEEE Transactions on Power Systems*, 33(6):6501–6509, 2018.

- [61] T. Xu, A. B Birchfield, K. S Shetye, and T. J Overbye. Creation of synthetic electric grid models for transient stability studies. In *IREP Symposium Bulk Power System Dynamics and Control*, 2017.
- [62] T. Xu, Y. Liu, and T. J. Overbye. Metric development for evaluating inertia's locational impacts on system primary frequency response. pages 1–6, Feb 2018.
- [63] Y. Yang and A. E. Motter. Cascading failures as continuous phase-space transitions. *Phys. Rev. Lett.*, 119(24):248–302, 2017.
- [64] R. D. Zimmerman, C. E. Murillo-Sánchez, and R. J. Thomas. Matpower: Steady-state operations, planning and analysis tools for power systems research and education. *Power Systems, IEEE Transactions*, 26:12–19, 2011.